

# Temporal-Prior-Guided View Planning for Periodic 3D Plant Reconstruction

Sicong Pan

Xuying Huang

Maren Bennewitz

**Abstract**—Periodic 3D reconstruction is essential for crop monitoring, but costly when each cycle restarts from scratch, wasting resources and ignoring information from previous captures. We propose temporal-prior-guided view planning for periodic plant reconstruction, in which a previously reconstructed model of the same plant is non-rigidly aligned to a new partial observation to form an approximation of the current geometry. To accommodate plant growth, we inflate this approximation and solve a set covering optimization problem to compute a minimal set of views. We integrated this method into a complete pipeline that acquires one additional next-best view before registration for robustness and then plans a globally shortest path to connect the planned set of views and outputs the best view sequence. Experiments on maize and tomato under hemisphere and sphere view spaces show that our system maintains or improves surface coverage while requiring fewer views and comparable movement cost compared to state-of-the-art baselines.

## I. INTRODUCTION

Monitoring the growth of crops is essential but labor-intensive. Autonomous monitoring with robots offers a scalable alternative, and recent work has explored active perception for 3D plant reconstruction by solving the next-best-view (NBV) planning problem [3, 6, 18, 27] to mitigate occlusions caused by complex plant structures. In production environments such as glasshouses, reconstruction needs to be carried out periodically (e.g., twice per week) to capture the continuous growth of plants. Most existing systems, however, restart the reconstruction process from scratch at each cycle, leading to unnecessary resource consumption and the loss of valuable information from previous captures.

Given a previously reconstructed 3D model of the same plant, how can we exploit this temporal prior to improve view planning for the current cycle? Our approach leverages two ideas. First, we perform non-rigid registration to align the prior model to a new partial observation, yielding an approximation of the current geometry on which we can plan directly, as shown in Fig. 1. Second, once a geometry approximation is available, we adopt a one-shot view planning strategy that computes a set of informative views at once by solving a set covering optimization problem balancing coverage and acquisition effort, following the spirit of [21].

Concretely, we follow the combined view planning pipeline in [22], which couples an initial NBV stage with

S. Pan, X. Huang, and M. Bennewitz are with the Humanoid Robots Lab at the University of Bonn, the Lamarr Institute for Machine Learning and Artificial Intelligence, and the Center for Robotics, University of Bonn, Germany. This work has partially been funded by the Deutsche Forschungsgemeinschaft (DFG, German Research Foundation) under grant 459376902 – AID4Crops, under Germany’s Excellence Strategy, EXC-2070 – 390732324 – PhenoRob, and by the BMBF within the Robotics Institute Germany, grant No. 16ME0999.

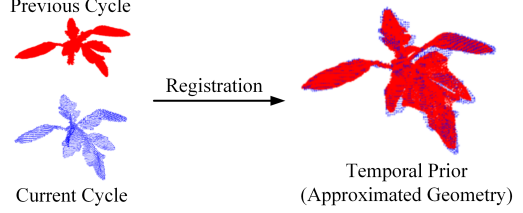


Fig. 1: An example of the temporal prior construction for the target maize plant. The full 3D reconstruction from the previous cycle (red) and the partial observation acquired in the current cycle (blue) are registered to generate an approximated geometry, which serves as a temporal prior for subsequent view planning.

one-shot planning. In practice, a single extra NBV typically increases the observed surface to about 60–80% (see [22]), which is adequate for robust non-rigid registration. After registration, we account for potential plant growth between acquisition cycles by introducing an inflation step to the approximated geometry. The inflated geometry approximation then serves as the input to the set covering optimization to compute the minimal view set for the current cycle.

To the best of our knowledge, this is the first work to leverage temporal priors of growing plants to enhance view planning for periodic 3D reconstruction. Our contributions are summarized as follows:

- Formalization of temporal-prior-guided view planning. Given a prior plant model and a new partial observation, plan a minimal view set that fully covers an inflated geometry approximation of the current plant.
- A complete pipeline that accounts for non-rigid registration robustness and potential plant growth across acquisition cycles.
- Experimental results demonstrate that our method maintains high reconstruction quality while reducing both the number of views and the robot’s movement cost compared with [20]. Moreover, it exhibits stronger generalization across varying plant complexities and view space configurations than [22].

To facilitate reproducibility, we release our implementation at <https://github.com/HumanoidsBonn/TPVP>.

## II. RELATED WORK

### A. View Planning in 3D Reconstruction

3D reconstruction is central to many robotic applications. Without prior knowledge, a common approach is NBV planning: iteratively select the next camera pose from the current reconstruction to greedily maximize information gain, using either search-based [3, 18, 19, 27] or learning-based [5, 6,

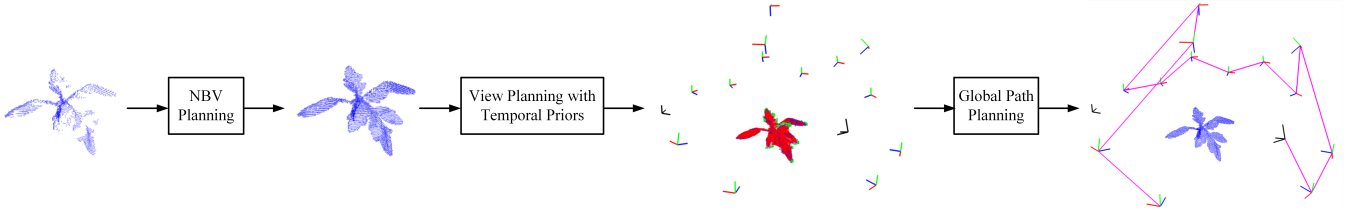


Fig. 2: Overview of the proposed view planning pipeline, following the combined framework in [22]. The system starts from a random initial view to acquire an initial point cloud, which is then fused with a subsequent observation planned by the NBV module. Using temporal priors, it predicts the minimum set of views required to cover the plant to be reconstructed. Planned views are visualized with their local coordinate axes in red, green, and blue—while the initial view and NBV are indicated in black. Finally, the global path (purple) is computed to minimize the robot’s movement cost during data collection.

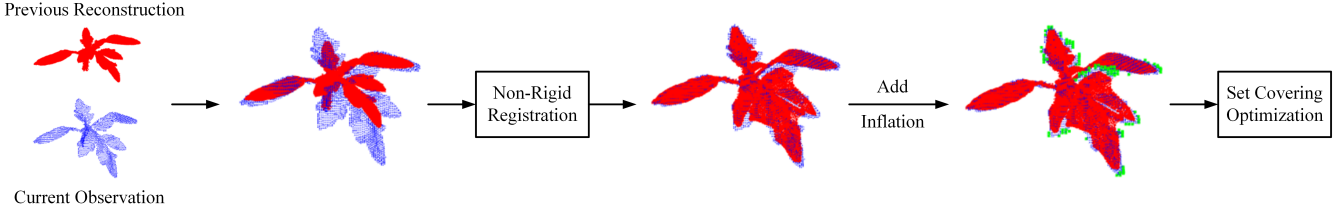


Fig. 3: Detailed pipeline of view planning with temporal priors. The framework first aligns the previously reconstructed 3D point cloud of the same plant (red)—serving as the temporal prior—with the current observation from the initial view and NBV (blue) via non-rigid registration. It then applies inflation (green) to account for potential plant growth. Finally, a set covering optimization problem is solved to determine the minimum view set required to fully cover the inflated geometry approximation.

17, 28] techniques. While effective, NBV requires expensive online map updates and often yields inefficient trajectories.

To mitigate this, one-shot view planning [11, 21, 23, 24] predicts the entire set of required views from an initial measurement and then computes a globally short path through them, substantially reducing movement cost. A recent system [22] combines NBV with one-shot planning—using a single NBV to activate a trained network from the set-covering-based view planning dataset—thereby preserving reconstruction quality while reducing movement cost.

However, these pipelines typically depend on learned shape priors trained on generic object datasets, which are not specific to agricultural settings. Our approach replaces such learned priors with temporal priors: we reuse the previous-cycle reconstruction of the same plant to guide view selection within the same combined pipeline. This preserves the efficiency benefits of the framework while making the prior plant-specific and periodic.

### B. Non-Rigid Registration

Non-rigid registration has been extensively surveyed [7]. Its goal is to align a source shape (mesh or point cloud) to a target observation. Unlike computer-graphics settings that often assume complete and well-defined shapes, robotic sensing needs to cope with noise and partial observations.

Many methods extend the rigid ICP paradigm and solve for a deformation using iterative nearest-neighbor matching with regularization (e.g., optimal-step nonrigid ICP [2]). However, NN-based correspondences can become unstable under low overlap or large deformations. An alternative is to cast deformation on a graph and optimize node-wise rigid motions, as in embedded deformation [26]. This idea has recently been applied to spatio-temporal plant mapping in

the wild [15]. We follow the deformation graph formulation but tailor it to our single-plant point clouds.

Prior work primarily targets offline alignment of recorded data; in contrast, we use the registered (and inflated) geometry approximation online to inform view planning within a combined pipeline for efficient periodic plant reconstruction.

## III. OUR APPROACH

Our system pipeline is illustrated in Fig. 2. Following [22], we employ PC-NBV [28] for next-best-view selection, and solve a shortest Hamiltonian path problem [9] for global path planning for connecting selected views.

The detailed pipeline of our view planning module with temporal priors is shown in Fig. 3. This stage involves two key optimization problems: (i) Non-rigid registration to align the previous cycle’s reconstruction with the current partial observation, accounting for plant deformation; and (ii) Set-covering optimization to determine the minimal set of views needed to cover the inflated geometry approximation.

### A. Non-Rigid Registration with Temporal Priors

We assume the target plant remains at the same physical location across cycles, so the previous reconstruction and the current observation share a common global frame and can be fused directly.

Let the previous-cycle source point cloud be  $\mathcal{P} = \{p_i\}_{i=1}^N$  (complete model) and the current partial observation be  $\mathcal{Q}$ . We seek a non-rigid warp that aligns  $\mathcal{P}$  to  $\mathcal{Q}$  and yields the geometry approximation  $\tilde{\mathcal{P}} = \{\tilde{p}_i\}$  for subsequent view planning.

We build an embedded deformation (ED) graph [26] on  $\mathcal{P}$  by voxel down-sampling (voxel size 0.004 m). Graph nodes

are voxel centers  $\{n_j\}$  with edges linking  $k$ -nearest neighbors. Each point  $p_i$  is softly attached to its  $K_a$  nearest graph nodes (anchors;  $K_a=8$ ) with weights  $w_{ij}$  computed from the point–node distances via a Gaussian decaying kernel and normalized per point to sum to one. The warped position is the standard ED blend of per-node rigid transforms:

$$\tilde{p}_i = \sum_{n_j \in \mathcal{A}(i)} w_{ij} \left( R_j(p_i - n_j) + n_j + t_j \right), \quad (1)$$

where  $R_j \in \text{SO}(3)$  and  $t_j \in \mathbb{R}^3$  are, respectively, the rotation and translation parameters of node  $n_j$ , and  $\mathcal{A}(i)$  denotes the anchor set of  $p_i$ .

We minimize a weighted sum of three standard terms:

$$\mathcal{L} = \lambda_{\text{arap}} \mathcal{L}_{\text{arap}} + \lambda_{\text{cd}} \mathcal{L}_{\text{cd}} + \lambda_{\text{lap}} \mathcal{L}_{\text{lap}} \quad (2)$$

Here  $\mathcal{L}_{\text{arap}}$  is the ED as-rigid-as-possible regularizer on the graph [26].  $\mathcal{L}_{\text{cd}}$  is the symmetric Chamfer distance between  $\tilde{\mathcal{P}}$  and  $\mathcal{Q}$  robust for partial scans without explicit correspondences.  $\mathcal{L}_{\text{lap}}$  is a sampled first-order Laplacian smoothness on  $\tilde{\mathcal{P}}$ , encouraging local geometric continuity in the complete prior. We set  $(\lambda_{\text{arap}}, \lambda_{\text{cd}}, \lambda_{\text{lap}}) = (1.0, 0.1, 0.01)$  to emphasize the as-rigid-as-possible term while keeping the Chamfer and Laplacian terms as mild regularizers to balance fidelity and smoothness.

Rotations are updated on  $\text{SO}(3)$  via the exponential map. We use Adam [13] with a learning rate of 0.1 for 300 iterations. The aligned point cloud  $\tilde{\mathcal{P}}$  is then used by the subsequent set covering optimization stage.

### B. Set Covering Optimization with Inflated Approximation

To capture likely growth regions, we augment the aligned prior  $\tilde{\mathcal{P}}$  with an inflation set  $\mathcal{I}$  consisting of points that are near the current scan and far from the prior. A candidate point is accepted if its 1-NN distance to  $\mathcal{Q}$  is less than  $\gamma_{\text{near}} = 0.003$  m and its 1-NN distance to  $\tilde{\mathcal{P}}$  exceeds  $\gamma_{\text{far}} = 0.005$  m. Distances are computed via KD-tree nearest-neighbor queries, and candidates are generated on a voxel grid with resolution 0.004 m.

Because the subsequent set covering step uses ray casting for visibility checks, we also include  $\mathcal{Q}$  in the approximation to prevent rays from penetrating already observed surfaces. We therefore construct the inflated geometry approximation used for set covering as the union  $\tilde{\mathcal{P}}^+ = \tilde{\mathcal{P}} \cup \mathcal{Q} \cup \mathcal{I}$ .

To make the optimization efficient, we build a sparse surface representation of the inflated approximation  $\tilde{\mathcal{P}}^+$ . Concretely, we ray-cast and voxelize the approximation with OctoMap [10] at a voxel resolution of 0.004 m to obtain a set of surface points  $\mathcal{P}_{\text{surf}} = \{p_i\}$ .

Let  $\mathcal{V} \subset \mathbb{R}^3 \times \text{SO}(3)$  be a discrete set of candidate views (e.g., hemisphere or sphere configurations with a radius of 0.4 m, as detailed in Sec. IV). For each  $v \in \mathcal{V}$ , visibility is computed by OctoMap ray casting to produce the visible set  $\mathcal{P}_v \subseteq \mathcal{P}_{\text{surf}}$ . We define the indicator:

$$I(p, v) = \begin{cases} 1, & \text{if } p \in \mathcal{P}_v, \\ 0, & \text{otherwise.} \end{cases} \quad (3)$$

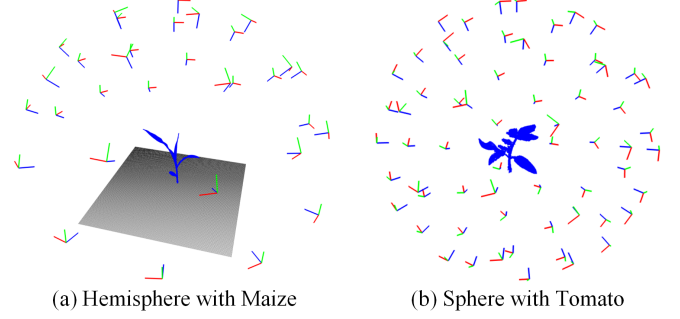


Fig. 4: Examples of the two environmental configurations used in our experiments. (a) Hemisphere view space with a supporting table, shown with a Maize plant. (b) Sphere view space without a table, shown with a Tomato plant.

We then solve a set covering optimization problem to select the minimum number of views that fully cover the surface points:

$$\begin{aligned} \min_{\{x_v\}} \quad & \sum_{v \in \mathcal{V}} x_v \\ \text{s.t.} \quad & \sum_{v \in \mathcal{V}} I(p, v) x_v \geq 1, \quad \forall p \in \mathcal{P}_{\text{surf}}, \\ & x_v \in \{0, 1\}, \quad \forall v \in \mathcal{V}. \end{aligned} \quad (4)$$

Here  $x_v$  is a binary decision variable indicating whether view  $v$  is selected, and  $\sum_{v \in \mathcal{V}} I(p, v) x_v \geq 1$  enforces that every surface point  $p \in \mathcal{P}_{\text{surf}}$  must be covered by at least one chosen view that observes this point.

This formulation is an integer linear program and is solved with Gurobi [8]. Note that the initial view and the NBV are already visited; therefore, they are excluded from the optimization along with their corresponding surface points, and the solver is applied to select additional views that cover the remaining surface. The resulting view set is then passed to the global path planner.

All of the implementation parameters above are chosen with respect to the overall plant size, which is normalized to 0.12 m (to fit the simulation platform in [22]). In practice, the voxel size should be selected to balance the number of optimization variables with the desired computational speed. Further implementation details and exact parameter values can be found in our released code.

## IV. EXPERIMENTAL RESULTS

**Dataset and Test Platform.** To evaluate periodic 3D plant reconstruction, we adopt real growing-plant data from [4] for non-rigid, cross-cycle registration on maize and tomato. The dataset contains two plant types (maize and tomato), each with three plant instances. For each instance, we use the last two consecutive time steps, as later growth stages are more complex and thus provide a more challenging test setup for view planning performance. Since view planning algorithms are usually sensitive to the initial observation, following [22], we evaluate two global rotations ( $0^\circ$  and  $45^\circ$ ) and three initial viewpoints (near-horizontal, oblique, and near-top). In total, this yields  $2 \times 3 \times 2 \times 3 = 36$  test cases.

View Space	Method	Number of Views	Surface Coverage (%)	Movement Cost (m)
Hemisphere	GMC [20]	5	91.12 $\pm$ 3.12	<b>2.05</b> $\pm$ 0.38
		10	97.71 $\pm$ 0.83	4.54 $\pm$ 0.67
		15	98.67 $\pm$ 0.50	6.02 $\pm$ 0.97
		20	<b>99.11</b> $\pm$ 0.53	7.17 $\pm$ 1.04
	MA-SCVP [22]	12.61 $\pm$ 1.20	98.80 $\pm$ 0.43	3.05 $\pm$ 0.30
	Ours	11.06 $\pm$ 3.38	98.77 $\pm$ 0.91	3.10 $\pm$ 0.51
Sphere	GMC [20]	5	81.86 $\pm$ 11.13	<b>1.77</b> $\pm$ 0.51
		10	90.58 $\pm$ 10.25	4.21 $\pm$ 0.82
		15	95.18 $\pm$ 5.84	6.75 $\pm$ 1.04
		20	97.14 $\pm$ 3.63	9.21 $\pm$ 1.26
	MA-SCVP [22]	12.72 $\pm$ 1.09	92.92 $\pm$ 4.29	2.99 $\pm$ 0.22
	Ours	9.22 $\pm$ 1.66	<b>98.44</b> $\pm$ 0.68	3.35 $\pm$ 0.41

TABLE I: View planning performance under different view space configurations for various methods. Note that GMC selects the NBV iteratively, so results are reported for 5, 10, 15, and 20 views to show overall performance, whereas MA-SCVP and our method predict the required number of views for each test case directly.

**View Space Configuration.** The view planning simulator in [22] assumes a tabletop setting with a hemispherical view space of 32 views. In real production settings, the feasible view space can change dynamically due to robot reachability and occlusions. We therefore additionally evaluate a more flexible spherical view space of 63 views. These views are evenly distributed around the target object by solving the Tamms problem [14]. Conceptually, this is aligned with multi-elevation, multi-view capture setups seen in recent plant-phenotyping systems [1], without attempting to replicate any specific hardware. Fig. 4 illustrates both configurations.

**Baseline and Evaluation.** We compare against the best-performing NBV method, GMC [20], and the combined method MA-SCVP [22], both reported in [22]. GMC is an NBV-based approach that iteratively selects the most informative next view for data collection, while MA-SCVP uses learned priors in its network for set-covering view planning. Following [22], we report three metrics: (i) the number of views required to complete the reconstruction, (ii) the visible surface coverage, defined as the ratio of reconstructed points to all visible points from the entire view space, and (iii) the movement cost, measured as the accumulated Euclidean path length connecting all selected views.

#### A. Evaluation of View Planning Performance

In this section, we analyze the view planning performance across different methods under varying view space configurations. As shown in Table I, our method maintains high reconstruction quality while reducing the required resources in terms of both the number of views and the associated movement cost.

**Comparison to NBV-Based GMC.** While GMC achieves higher surface coverage as the number of viewpoints increases, this improvement comes at the cost of substantially increased robot movement and more viewpoints. In contrast, our method offers a more favorable trade-off between surface coverage performance and reconstruction efficiency.

**Comparison to Combined Pipeline MA-SCVP.** Our method achieves near-complete surface coverage with fewer

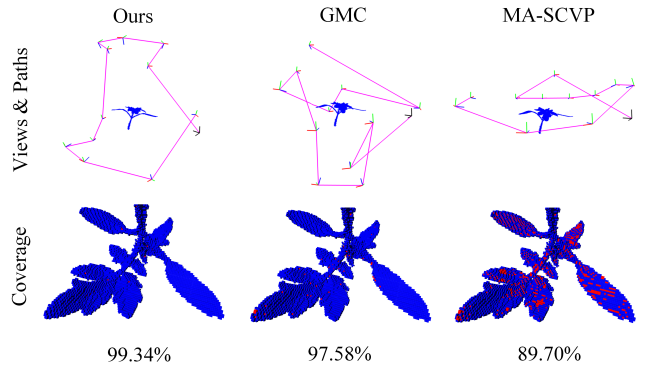


Fig. 5: Visual comparison of our method with GMC [20] and MA-SCVP [22]. The top row shows the same initial view (black), the selected views (red-green-blue), and the corresponding view paths (purple). For a fair comparison, all methods are visualized with 12 views (our method and MA-SCVP both predict 12 views, while 12 views are selected from GMC for consistency). The bottom row visualizes the reconstructed plant surfaces (blue) and uncovered regions (red) using voxelization, focusing on the bottom part of the plant. Our method achieves the highest surface coverage with a shorter path; GMC also attains good coverage but with a longer path; MA-SCVP, despite a similar path length, fails to observe the bottom surface details.

views than MA-SCVP, reflecting a more complexity-aware, object-specific allocation of the viewpoint budget. In terms of view space generalization, unlike MA-SCVP—whose network is trained on and limited to a fixed 32-pose hemisphere and thus cannot include bottom views—our method adapts to flexible view space configurations. In the sphere setting, our method considers bottom views and also achieves near-complete surface coverage. To illustrate this, we present in Fig. 5 a visualization of a representative reconstruction example. Overall, this adaptability allows our approach to maintain high performance across diverse plant types and varying view space constraints, both of which can change dynamically in real production environments.

**Time Analysis.** The mission time of a reconstruction run is dominated by three factors: (i) the number of views to acquire and fuse, (ii) the robot movement between views, and (iii) the planner’s inference time. On our setup, planner inference takes 10–15 seconds for our method, less than 1 second for MA-SCVP, and about 1.5 seconds per iteration for GMC (about 30 seconds for 20 views). Because our method typically requires fewer views and induces less movement cost than GMC, the overall mission time is lower despite comparable inference time. Compared to MA-SCVP, our inference time is higher (with similar movement cost and a slightly smaller number of views), so the overall mission time can be longer. We argue this overhead is justified by improved coverage and flexibility: unlike MA-SCVP, our method adapts the view space and achieves near-complete coverage in the sphere configuration.

#### B. Ablation Study on Inflation

In this section, we present an ablation study on the impact of the inflation module, where only the aligned prior is retained for the set covering. As shown in Table II, in-

Plant Type	Method	Number of Views	Surface Coverage (%)	Movement Cost (m)
Maize	Ours w/o Inflation	6.75 $\pm$ 0.97	96.99 $\pm$ 1.16	2.51 $\pm$ 0.32
	Ours w/ Inflation	7.92 $\pm$ 1.02	<b>98.06 <math>\pm</math> 0.75</b>	2.85 $\pm$ 0.29
Tomato	Ours w/o Inflation	11.42 $\pm$ 2.05	98.98 $\pm$ 0.50	3.38 $\pm$ 0.30
	Ours w/ Inflation	12.37 $\pm$ 2.17	<b>99.15 <math>\pm</math> 0.40</b>	3.61 $\pm$ 0.28

TABLE II: Ablation study evaluating the impact of geometry approximation inflation on view planning performance.

Plant Type	View Space	Number of Views	Surface Coverage (%)
Maize	Hemisphere	7.94 $\pm$ 1.11	98.09 $\pm$ 0.82
	Sphere	<b>7.89 <math>\pm</math> 0.96</b>	98.02 $\pm$ 0.69
Tomato	Hemisphere	14.17 $\pm$ 1.34	99.45 $\pm$ 0.20
	Sphere	<b>10.56 <math>\pm</math> 0.98</b>	98.85 $\pm$ 0.32

TABLE III: Performance of our method across different plant types and view space configurations.

corporating inflation consistently improves surface coverage compared to the no-inflation variant across both plant types. The improvement is particularly notable for maize, which we attribute to inflation’s ability to compensate for slight registration errors and account for inter-cycle growth between the current observations and the predicted deformation, thereby leading to better coverage performance in such cases.

### C. Analysis on Plant Complexity

In this section, we evaluate our method across different view space configurations and plant types, which correspond to different levels of structural complexity. As shown in Table III, our method assigns fewer views to the simpler plant (maize) and more to the more complex plant (tomato), consistent with their occlusion patterns—tomato’s broad leaves incur heavier self-occlusion. Moreover, for the tomato, we require fewer views in the sphere configuration than in the hemisphere configuration, because bottom occlusions are easier to resolve when viewpoints are allowed below the plant. Taken together, these results indicate that our method adaptively allocates the viewpoint budget according to plant complexity and the available view space.

### D. Analysis on NBV Module

In this section, we analyze the effect of the NBV module by computing the Chamfer distance between the aligned priors and the ground truth. As shown in Table IV, introducing a single NBV consistently reduces the Chamfer distance compared with using only the initial view. This indicates that without the NBV, the non-rigid registration is less reliable and more prone to errors. Moreover, when relying solely on the initial view (without inflation), the final reconstruction surface coverage decreases to  $97.61 \pm 1.75$ , averaged over both the hemisphere and sphere. These results demonstrate that adding one NBV provides complementary information that enhances the robustness of non-rigid registration and ultimately improves the reconstruction quality.

## V. DISCUSSION

In this work, we use real growing-plant data [4] with non-rigid, cross-cycle registration as an approximation for

Method	Chamfer Distance (mm)
Initial View Only	2.764 $\pm$ 1.195
Initial View + One NBV	<b>1.743 <math>\pm</math> 0.444</b>

TABLE IV: Registration performance when using only the initial view or adding one NBV.

deployment in production environments such as glasshouses. Moving toward a deployable robotic system in the field, we identify one possible challenge: spatio-temporal mapping in real glasshouse deployments. Our current method assumes that non-rigid growth of a single plant between cycles remains within a range that allows reliable registration using partial observations. Larger and more irregular deformations of multiple plants in the glasshouse may violate this assumption, leading to registration drift and reduced view planning performance. Recent work on spatio-temporal consistent plant mapping has demonstrated robust localization and deformation handling in large unstructured environments [15], which represents a promising direction for future extension.

To move closer to deployment, we plan to integrate our approach with global view motion planning to account for the robot arm’s motion cost in joint space (approximated in this work using Euclidean distance, following [22]). Our temporal prior can directly replace static priors in global view motion planning frameworks for fruit and plant mapping, retaining set-covering-based coverage while benefiting from globally optimized paths [12].

Finally, considering semantic consistency across cycles may provide another direction to improve robustness. Semantic cues can serve as stable anchors for cross-cycle correspondence and guide view planning toward plant structures that are often occluded yet crucial for monitoring, such as fruits or peduncles. Leveraging annotated maize and tomato datasets for semantic evaluation [25], and building on spatio-temporal semantic mapping to maintain instance-level continuity over time [16], could further enhance performance.

## VI. CONCLUSION

We presented a temporal-prior-guided view planning approach integrated into a combined pipeline that couples an initial NBV stage with one-shot planning. Starting from a previous-cycle reconstruction, we acquire one additional NBV to obtain an informative observation and improve registration robustness, non-rigidly register the prior to the current partial reconstruction, inflate the geometry approximation to account for inter-cycle growth, and solve a set-covering problem to compute a minimal view set; the selected views are then sequenced by a global path planner. Experiments show that our method maintains or improves surface coverage while using fewer views and comparable robot movement, and it generalizes better to plant complexity and flexible view space configurations than strong baselines. These results highlight the value of temporal priors for periodic 3D plant reconstruction.

## REFERENCES

[1] S. Adebola, S. Xie, C. M. Kim, J. Kerr, B. M. van Marrewijk, M. van Vlaardingen, T. van Daalen, E. van Loo, J. L. S. Rincon, E. Solowjow *et al.*, “Growsplat: Constructing temporal digital twins of plants with gaussian splats,” *arXiv preprint arXiv:2505.10923*, 2025.

[2] B. Amberg, S. Romdhani, and T. Vetter, “Optimal step nonrigid icp algorithms for surface registration,” in *2007 IEEE conference on computer vision and pattern recognition*. IEEE, 2007, pp. 1–8.

[3] A. K. Burusa, E. J. van Henten, and G. Kootstra, “Attention-driven next-best-view planning for efficient reconstruction of plants and targeted plant parts,” *Biosystems Engineering*, 2024.

[4] N. Chebrolu, F. Magistri, T. Läbe, and C. Stachniss, “Registration of spatio-temporal point clouds of plants for phenotyping,” *PloS one*, vol. 16, no. 2, p. e0247243, 2021.

[5] X. Chen, Q. Li, T. Wang, T. Xue, and J. Pang, “Gennbv: Generalizable next-best-view policy for active 3d reconstruction,” in *Proceedings of the IEEE/CVF Conference on Computer Vision and Pattern Recognition*, 2024, pp. 16436–16445.

[6] J. Ci, E. J. van Henten, X. Wang, A. K. Burusa, and G. Kootstra, “Ssl-nbv: A self-supervised-learning-based next-best-view algorithm for efficient 3d plant reconstruction by a robot,” *Computers and Electronics in Agriculture*, vol. 233, p. 110121, 2025.

[7] B. Deng, Y. Yao, R. M. Dyke, and J. Zhang, “A survey of non-rigid 3d registration,” in *Computer Graphics Forum*, vol. 41, no. 2. Wiley Online Library, 2022, pp. 559–589.

[8] L. Gurobi Optimization, “Gurobi Optimizer Reference Manual,” 2021.

[9] M. Held and R. M. Karp, “A dynamic programming approach to sequencing problems,” *Journal of the Society for Industrial and Applied mathematics*, vol. 10, no. 1, pp. 196–210, 1962.

[10] A. Hornung, K. M. Wurm, M. Bennewitz, C. Stachniss, and W. Burgard, “OctoMap: An Efficient Probabilistic 3D Mapping Framework Based on Octrees,” *Autonomous Robots*, 2013.

[11] H. Hu, S. Pan, L. Jin, M. Popović, and M. Bennewitz, “Active Implicit Reconstruction Using One-Shot View Planning,” in *Proc. of the IEEE Intl. Conf. on Robotics & Automation (ICRA)*, 2024.

[12] A. I. Jose, S. Pan, T. Zaenker, R. Menon, S. Houben, and M. Bennewitz, “Go-vmp: Global optimization for view motion planning in fruit mapping,” *arXiv preprint arXiv:2503.03912*, 2025.

[13] D. P. Kingma and J. Ba, “Adam: A method for stochastic optimization,” *arXiv preprint arXiv:1412.6980*, 2014.

[14] X. Lai, D. Yue, J.-K. Hao, F. Glover, and Z. Lü, “Iterated dynamic neighborhood search for packing equal circles on a sphere,” *Computers & Operations Research*, vol. 151, p. 106121, 2023.

[15] L. Lobefaro, M. V. Malladi, T. Guadagnino, and C. Stachniss, “Spatiotemporal consistent mapping of growing plants for agricultural robots in the wild,” in *2024 IEEE/RSJ International Conference on Intelligent Robots and Systems (IROS)*. IEEE, 2024, pp. 6375–6382.

[16] L. Lobefaro, M. Sodano, D. Fusaro, F. Magistri, M. V. Malladi, T. Guadagnino, A. Pretto, and C. Stachniss, “Spatio-temporal consistent semantic mapping for robotics fruit growth monitoring,” *IEEE Robotics and Automation Letters*, 2025.

[17] M. Mendoza, J. I. Vasquez-Gomez, H. Taud, L. E. Sucar, and C. Reta, “Supervised Learning of the Next-Best-View for 3D Object Reconstruction,” *Pattern Recognition Letters*, vol. 133, pp. 224–231, 2020.

[18] R. Menon, T. Zaenker, N. Dengler, and M. Bennewitz, “NBV-SC: Next Best View Planning based on Shape Completion for Fruit Mapping and Reconstruction,” in *Proc. of the IEEE/RSJ Intl. Conf. on Intelligent Robots and Systems (IROS)*, 2023.

[19] S. Pan and H. Wei, “A Global Max-Flow-Based Multi-Resolution Next-Best-View Method for Reconstruction of 3D Unknown Objects,” *IEEE Robotics and Automation Letters (RA-L)*, vol. 7, no. 2, pp. 714–721, 2022.

[20] S. Pan and H. Wei, “A Global Generalized Maximum Coverage-Based Solution to the Non-Model-Based View Planning problem for object reconstruction,” *Journal of Computer Vision and Image Understanding (CVIU)*, vol. 226, p. 103585, 2023.

[21] S. Pan, H. Hu, and H. Wei, “SCVP: Learning One-Shot View Planning via Set Covering for Unknown Object Reconstruction,” *IEEE Robotics and Automation Letters (RA-L)*, 2022.

[22] S. Pan, H. Hu, H. Wei, N. Dengler, T. Zaenker, and M. Bennewitz, “Integrating one-shot view planning with a single next-best view via long-tail multiview sampling,” *IEEE Transactions on Robotics (T-RO)*, 2024.

[23] S. Pan, L. Jin, H. Hu, M. Popović, and M. Bennewitz, “How Many Views Are Needed to Reconstruct an Unknown Object Using NeRF?” in *Proc. of the IEEE Intl. Conf. on Robotics & Automation (ICRA)*, 2024.

[24] S. Pan, L. Jin, X. Huang, C. Stachniss, M. Popović, and M. Bennewitz, “Exploiting Priors from 3D Diffusion Models for RGB-Based One-Shot View Planning,” in *Proc. of the IEEE/RSJ Intl. Conf. on Intelligent Robots and Systems (IROS)*, 2024.

[25] D. Schunck, F. Magistri, R. A. Rosu, A. Cornelissen, N. Chebrolu, S. Paulus, J. Léon, S. Behnke, C. Stachniss, H. Kuhlmann *et al.*, “Pheno4d: A spatio-temporal dataset of maize and tomato plant point clouds for phenotyping and advanced plant analysis,” *Plos one*, vol. 16, no. 8, p. e0256340, 2021.

[26] R. W. Sumner, J. Schmid, and M. Pauly, “Embedded deformation for shape manipulation,” in *ACM siggraph 2007 papers*, 2007, pp. 80–es.

[27] T. Zaenker, C. Smitt, C. McCool, and M. Bennewitz, “Viewpoint planning for fruit size and position estimation,” in *Proc. of the IEEE/RSJ Intl. Conf. on Intelligent Robots and Systems (IROS)*, 2021.

[28] R. Zeng, W. Zhao, and Y.-J. Liu, “PC-NBV: A Point Cloud Based Deep Network for Efficient Next Best View Planning,” in *Proc. of the IEEE/RSJ Intl. Conf. on Intelligent Robots and Systems (IROS)*, 2020.